A SANS Study of the Conformational Behavior of Linear Chains in Compressed and Uncompressed End-Linked Elastomers

Nisha Gilra,[†] Claude Cohen,*,[†] Robert M. Briber,[‡] Barry J. Bauer,[§] Ronald C. Hedden,[†] and Athanassios Z. Panagiotopoulos[⊥,#]

School of Chemical Engineering, Cornell University, Ithaca, New York 14853; Department of Materials and Nuclear Engineering, University of Maryland, College Park, Maryland 20742; Polymers Division, National Institute of Standards and Technology, Gaithersburg, Maryland 20899; and Institute for Physical Science & Technology and Department of Chemical Engineering, University of Maryland, College Park, Maryland 20742

ABSTRACT: Small-angle neutron scattering (SANS) experiments were performed to determine the conformational behavior of unattached deuterated linear poly(dimethylsiloxane) (PDMS) chains of $M_n = 51\,000$ g mol^{-1} in uncompressed and compressed end-linked protonated PDMS networks with a minimal amount of defects. The networks were prepared from low-polydispersity precursor chains with $M_n = 9900$ g mol^{-1}, 34 800 g mol^{-1}, and 71 500 g mol^{-1}. The samples are hereafter labeled 10K, 35K, and 70K. The mixtures of the 10K network with the linear chains were prepared by cross-linking around the linear chains, while the 35K and 70K network systems were swollen with the linear chains after the network was formed. No significant variation of the radius of gyration of the linear chains was observed as a function of network mesh size, in agreement with recent Monte Carlo simulations. The results from the compressed 35K and 70K networks exhibited excess scattering at small wave vectors, indicating phase segregation, and they could not be quantitatively analyzed. The scattering data from the trapped chains in the compressed 10K networks were fitted well with a Kratky−Porod wormlike chain model, indicating segment alignment consistent with Monte Carlo simulations and deuterium NMR results.

1. Introduction and Background

Several researchers have used small-angle neutron scattering (SANS) to examine the radius of gyration, R_g, of linear polymer probe chains trapped in a polymer network, but the results have not been consistent. This problem is important as the conformation of a polymer molecule relates to its transport through membranes, gels, and other porous structures.[1,2] Boué et al.[3] conducted a SANS study of deuterated free linear poly(dimethylsiloxane) (PDMS) chains in a nondeuterated PDMS network. The length of the free chains was approximately the same as the length between cross-links of the network or mesh size (N_c). The free linear chains were allowed to diffuse into the networks and had a mass fraction of 9%. They observed that the R_g of the linear chains in the network was equivalent to the R_g of the same chains in a PDMS melt. On the other hand, Horkay et al.[4] investigated the conformation of a small volume fraction (0.22%) of linear poly(vinyl acetate) (PVAc) chains absorbed into a PVAc network swollen in isopropyl alcohol. The length of the free chains was comparable with the estimated mesh size, and they reported a decrease of 40% in R_g of the linear chains. These two studies reported results from only one mesh size. Liu et al.[1] studied protonated polystyrene (PS) networks containing deuterated linear PS with a broad range of mesh sizes. The PS networks were formed around the free PS chains. The volume fraction

of the linear chains varied from 2% to 5%. They determined that when the mesh size was greater than the degree of polymerization of the linear chain, N_1, R_g did not change appreciably. But when N_c became smaller than N_1, the R_g decreased according to the relation $R_g^{-1} \sim N_c^{-1}$. They also observed phase segregation during cross-linking of the samples with low mesh sizes. Because of the inconsistencies in the values of the radii of gyration of linear chains trapped in networks reported in previous works, a careful determination of the radius of gyration of such chains trapped in networks of different mesh size seems in order.

Another subject of interest is the alignment of an unattached probe chain in a strained polymer network. In their SANS study, Boué et al. did not observe any evidence of alignment of the free polymer chains trapped in a network that was uniaxially stretched. On the other hand, computer simulations suggest orientation alignment between the segments of the trapped chain and those of the network as well as strong orientation correlation (alignment) in neighboring segments of the trapped chain compared to the structure of the chain in undeformed networks or in the melt.[5−12] Also, extensive deuterium nuclear magnetic resonance (D NMR) experiments and birefringence experiments suggest orientation alignment of the segments of the trapped chains in a deformed network.[13−17] Other scattering experiments also provide evidence of induced deformation because they produce anisotropic isointensity scattering patterns, such as "butterfly" patterns.[18−21] Boué et al. suggested that because chain alignment is present only at short length scales, it was not detected by their SANS measurements. Their data did not go to large enough q vectors (i.e., small size scale) to detect segmental alignment. The scattering vector, q, is defined as

† Cornell University.

‡ Department of Materials and Nuclear Engineering, University of Maryland.

§ National Institute of Standards and Technology.

⊥ Institute for Physical Science & Technology and Department of Chemical Engineering, University of Maryland.

Current address: Department of Chemical Engineering, Princeton University, Princeton, NJ 08544.

$$q = \frac{4\pi}{\lambda} \sin(\theta/2) \qquad (1)$$

where λ is the incident neutron wavelength and θ is the scattering angle. Experiments going out to higher q vectors will be described in this work.

In this work, a SANS study of linear PDMS chains trapped in PDMS networks prepared with different molecular mass precursors is performed to investigate the behavior of the radius of gyration of the linear chain as a function of the network mesh size. Also, neutron scattering intensities at higher q ranges (smaller length scales) are measured to examine the effect of compression on the length scale of the individual segments of the probe chains. The networks used are prepared at the optimal ratio of cross-links to precursor chains that produces the lowest soluble fractions and the highest modulus. This kind of network has been shown to have a minimal amount of structural defects.[22-24]

The scattering from a deuterated linear polymer chain in a hydrogenated polymer network has been shown by Liu et al.[1] to be consistent with the classical Zimm equation that describes the scattering from a dilute mixture of a linear polymer in a solvent

$$\frac{k_n \phi_1}{I(q)} = \frac{1}{v_1 N_1 P_1(q)} + 2 A_2 \phi_1 \qquad (2)$$

where $I(q)$ is the experimentally measured scattering intensity, ϕ_1 is the volume fraction of the linear chain, v_1 is the molar volume of the linear chain repeat unit, N_1 is the number-average degree of polymerization of the linear chain, $P_1(q)$ is the single-chain form factor, k_n is the neutron scattering contrast factor, and A_2 is the second virial coefficient. For a dilute mixture of the linear polymer chain in the polymer network, A_2 is given by

$$A_2 = \frac{3}{4 v_c N_c} - \frac{\chi}{v_0} \qquad (3)$$

where χ is the Flory–Huggins interaction parameter, v_c is the molar volume of the network repeat unit, and v_0 is the reference volume for the lattice [usually $v_0 = (v_1 v_c)^{1/2}$].[1] In the limit of infinite dilution ($\phi_1 \to 0$), the effect of A_2 is eliminated, generating the following relation for the single-chain form factor

$$\lim_{\phi_1 \to 0} \left[\frac{I(q)}{k_n \phi_1} \right] = v_1 N_1 P_1(q) \qquad (4)$$

For a polydisperse Gaussian polymer with a Zimm–Schultz molecular mass distribution,[25] $P_1(q)$ is given by a modified Debye function[26]

$$P_{1,P}(q) = \frac{2}{u^2} \left[u - 1 + \left[\frac{h}{h+u} \right]^h \right] \qquad (5)$$

with

$$h = \frac{1}{d-1} \qquad (6)$$

where d is the polydispersity index and

$$u = \langle R_g^2 \rangle q^2 \qquad (7)$$

where $\langle R_g^2 \rangle$ is the mean-squared radius of gyration. For

a Gaussian polymer chain, R_g^2 is

$$R_g^2 = \frac{N l^2}{6} \qquad (8)$$

where l is the statistical segment length.

For polymer chains that do not follow the linear chain Gaussian behavior, such as rings, stars, and rods, other single-chain form factors have been developed.[27] Of particular interest here is a form factor that has been developed for semiflexible wormlike chains that exhibit characteristics of both a flexible Gaussian chain and a rigid rod. A brief description of this model, known as the Kratky–Porod wormlike chain model,[28] is presented in the Appendix.

To characterize the deuterated linear chains, we performed SANS experiments on blends of deuterated and protonated linear chains. The scattering from a binary blend of linear polymers can be modeled using the random phase approximation (RPA) developed by de Gennes[29] and expressed as

$$\frac{k_n}{I(q)} = \frac{1}{N_1 v_1 \phi_1 P_1(q)} + \frac{1}{N_2 v_2 \phi_2 P_2(q)} - 2 \frac{\chi}{v_0} \qquad (9)$$

where subscript 2 refers to the properties of the non-deuterated polymer.

2. Experimental Procedures

2.1. Samples. Three series of end-linked poly(dimethylsiloxane) (PDMS) network samples with a minimal amount of defects and varying mesh sizes containing deuterated linear PDMS probe chains were studied. The precursor PDMS chains that constituted these three series of networks had molecular masses of M_n = 9900 g mol^{-1}, 34 800 g mol^{-1}, and 71 500 g mol^{-1} as listed in Table 1. A polystyrene equivalent molar mass was first obtained from gel permeation chromatography (GPC) and converted into the values reported in Table 1 using an established empirical correlation for PDMS.[30] In all series, the linear probe chains were 100% deuterated and had an absolute weight-average molar mass M_w = 59 700 g mol^{-1} determined from neutron scattering Zimm plots. The polydispersity of the linear probe chains was determined by GPC to be 1.17. The mass fractions of the probe chains in the networks were measured by deuterium NMR and ranged from approximately 1.0% to 5.7%, with the exception of sample 70K-2 that contained no deuterated material. The network samples were disk shaped with a thickness of approximately 0.1 cm. The 35K and 70K series were prepared by allowing the linear chains to diffuse into the network, while the 10K series were prepared by cross-linking the networks around the probe chains. The latter preparation was used to avoid the extremely long time needed for the probe chains to diffuse and homogenize in the 10K samples. The volume fractions of all of the samples studied were found to lie in the one-phase region close to a calculated equilibrium swelling curve of a PDMS network in a melt of linear PDMS chains.[31,32]

Two series of polymer blends denoted as 10KB and 70KB were also studied. The blends were made with the M_n = 51 000 g mol^{-1} probe chains mixed with either M_n = 9900 g mol^{-1} or 71 500 g mol^{-1} precursor PDMS chains. A detailed description of the samples used is shown in Table 2.

2.1.1. Compression. To study the effects of deformation on the probe chains in the networks, some of the samples were compressed. Samples 70K-5, 35K-3, 35K-5, 10K-1, and 10K-2 were compressed, and the amount of compression for each sample is shown in Table 2. Sample 35K-5 was compressed twice and labeled 35KC-5a and 35KC-5b; i.e., the sample was compressed once, its scattering was measured, and then the sample was compressed further and its scattering measured again.

Table 1. Molecular Mass (M_n) and Polydispersity (d) Characteristics of the Protonated PDMS Network Precursor Chains and Deuterated PDMS Linear, Probe Chains; the Elastic Modulus (G_e/RT) Is of the Corresponding PDMS Networks (See Text for Uncertainties)

sample	M_n (10^3 g mol^{-1})	d	G_e/RT (mol/m^3)
10K	9.9	1.31	127.8
35K	34.8	1.3	88.0
70K	71.5	1.29	51.1
probe chain	51.0	1.17	

Table 2. Three Network Series (10K, 35K, 70K) and Two Blend Series (10KB and 70KB) Examined with SANS Experiments[a]

uncompressed sample	compressed sample	ϕ_1	% compression
10K-1	10KC-1	0.010	18
10K-2	10KC-2	0.005	26
35K-1		0.010	
35K-2		0.023	
35K-3	35KC-3	0.037	14
35K-4		0.018	
35K-5	35KC-5a	0.057	28
	35KC-5b	0.057	31
70K-2		0.000	
70K-4		0.038	
70K-5	70KC-5	0.057	34
10KB-1		0.010	
10KB-2		0.005	
70KB-1		0.186	

[a] The uncompressed sample label is in the left column, the compressed sample label is in the second column, the volume fraction of the linear chains is ϕ_1, and the amount of compression is in the last column.

A sample was compressed by placing it between two quartz windows that had been lubricated with a small amount of low molecular mass hydrogenous PDMS. These plates were then placed in a cylindrical brass cell in between two fittings that could be tightened, which in turn imparted a compressive force on the sample. The amount of compression was determined by measuring the difference in the thickness of the sample before and after compression. Also, the sample diameter was determined before and after compression. As a consistency check, the ratio of the cross-sectional area before and after compression was compared to the ratio of the thickness after and before compression and were found to be in good agreement. The samples were assumed to be uniformly compressed, although uneven threads in the brass cell could have led to some nonuniformity.

In Table 1, the uncertainty in the values of G_e/RT is approximately ± 1 mol/m^3. In Table 2, the uncertainty in the values of ϕ_1 is ± 0.002, and the relative uncertainty in the amounts of compression is $\pm 1\%$. All uncertainties are one standard deviation.

2.2. SANS Measurements. The neutron scattering experiments were performed at the Cold Neutron Research Facility (CNRF) at the National Institute of Standards and Technology (NIST).[33] The NIST 30 m SANS instrument was used for the 35K, 70K, and 70KB series, and the 8 m SANS instrument was used for the 10K and 10KB series. The incident neutron wavelength was 6 Å with a wavelength resolution $\Delta\lambda/\lambda = 0.15$ on the 30 m instrument and 5 Å with $\Delta\lambda/\lambda = 0.20$ on the 8 m instrument. A two-dimensional detector was used to collect the scattering data, and the scattering was performed at room temperature. The scattering intensity was corrected for background scattering, sample transmission and thickness, empty cell scattering, and detector efficiency. The intensity was placed on an absolute scale using standards calibrated at NIST. The standards used for the 70K network, 35K network, and 70KB blend samples were water, silica, and polystyrene. The standard used for the 10K network and 10KB blend samples was water. The data were radially averaged and reduced to $I(q)$ vs q form.

Table 3. Values of Incoherent Scattering (See Text for Uncertainties)

sample	I_i (cm^{-1})	sample	I_i (cm^{-1})
10K-1	0.611	70K-2	0.630
10K-2	0.624	70K-4	0.606
35K-1	0.624	70K-5	0.594
35K-2	0.616	10KB-1	0.603
35K-3	0.607	10KB-2	0.614
35K-4	0.619	70KB-1	0.592
35K-5	0.594		

Last, the scattering data were corrected for incoherent scattering. The incoherent scattering was calculated on the basis of the small fraction of deuterated material in the samples and an appropriately weighted profile following a procedure in Higgins and Benoît.[34] The value of I_i^H, the incoherent scattering from a sample of pure hydrogenous chains, was determined to be 0.63 cm^{-1} from the average of the medium- and high-q scattering of the blank sample, 70K-2. For the 10K samples, the incoherent scattering was extracted from a linear least-squares fit of the high-q regime according to the relationship[34]

$$I(q)q^2 = K + I_i q^2 \tag{10}$$

where K is a constant. The scattering of the compressed samples was corrected with the incoherent scattering calculated from the corresponding uncompressed samples. The values of the calculated incoherent scattering for each sample are shown in Table 3. All measurements have an uncertainty of approximately 0.001$-$0.004 cm^{-1}.

The uncertainties in the scattering data are calculated as the estimated standard deviation of the mean, and the total combined uncertainty is not given as comparisons are made with data obtained under the same conditions. In cases where the limits are smaller than the plotted symbols, the limits are left out for clarity. Standard error propagation was used to determine the uncertainties in the scattering intensity after the incoherent scattering was subtracted. The uncertainty in the intensity at high-q values is greater than the uncertainty at low-q values because there is increased uncertainty in the experimental measurement as q is increased. As will be seen in the results to be presented, this increased uncertainty becomes even more pronounced with increasing q when it is applied to the data of $I(q)q^2$ in the Kratky representation. Fits of the scattering data are made by a least-squares fit of the data, giving an average and a standard deviation to the fit. For the fits, the relative uncertainties are one standard deviation, based on the goodness of the fit.

3. Results and Discussion

3.1. Determination of the Radius of Gyration. To determine the radius of gyration of the probe chains in the uncompressed networks, the experimental scattering data were extrapolated to the limit of infinite dilution ($\phi_1 \rightarrow 0$). This method is also used for the 10KB blend samples. The extrapolation is carried out by using eq 1 and plotting $\phi_1/I(q)$ vs ϕ_1 for each q value. Then, a least-squares line is fit through the data for each q value. The y-intercept of each of these lines is then the $\phi_1/I(q)$ value that corresponds to the limit as $\phi_1 \rightarrow 0$. Then, eq 4 can be used to determine the single-chain form factor from which the radius of gyration can be extracted using eq 5.

To determine the single-chain form factors for each sample series, a program previously developed[35] was coupled with the NREG library, a series of FORTRAN programs used to perform nonlinear regression.[36] This program has a maximum of five variable parameters, of which two are generally kept fixed. The parameters are k_n, R_g, N_1, d, and the baseline. When using this

Table 4. N_1, R_g, and l As Determined by a Nonlinear Fit of the Scattering Data Extrapolated to Infinite Dilution.

series	N_1	R_g (Å)	l (Å)
10K	569.3 ± 8.3	60.8 ± 0.9	6.2 ± 0.1
35K	629.8 ± 3.1	65.0 ± 0.4	6.3 ± 0.1
70K	585.9 ± 5.4	60.8 ± 0.7	6.2 ± 0.1
10KB	577.6 ± 9.9	59.1 ± 1.1	6.0 ± 0.1

program, the neutron contrast factor k_n and the polydispersity index d are generally kept fixed.

The baseline can also be kept fixed if, for example, the incoherent scattering has already been subtracted off. If the degree of polymerization is known with certainty, it too can be kept fixed. N_1 can also be allowed to float when it is not known or when an independent verification is desired. Specifically, for this analysis, the baseline was fixed to equal 0, and N_1 and R_g were allowed to float. The best-fit values of the radius of gyration, degree of polymerization, and statistical segment length for all of the series are shown in Table 4, and the best fits for the 35K and 10KB series are shown in Figure 1.

The values of N_1 are in reasonable agreement with each other and fall within 10% of the value based on the absolute weight-average molar mass obtained from Zimm plots of the SANS data and the polydispersity measured using gel permeation chromatography (GPC). The fit values of the statistical segment length vary 7% to 12% from the literature value given to be $l =$ 5.61 Å.[37,38] The values of R_g obtained are also in very good agreement with the established relationship between R_g and M_w for PDMS in a Θ solvent[39]

$$R_{g,\Theta}/M_w{}^{0.5} = 0.25 \text{ Å/(g/mol)}^{0.5} \qquad (11)$$

For our probe chain with $M_w = 59\,700$ g mol^{-1}, one would obtain $R_g = 61$ Å from eq 11.

There does not appear to be a trend in the radius of gyration of the probe chains as the mesh size is increased. Monte Carlo simulations of probe chains of 50 repeat units immersed in a network of mesh size of 10 repeat units show that the R_g decreases only by approximately 6%.[40] Even if the R_g decreased on the order of 6% from one mesh size to another in these experiments, this small decrease falls in the range of experimental uncertainty. It thus appears that any variation in R_g as a function of mesh size in the range investigated is too small to be accurately detected. This is in agreement with the results of Boué et al.[3] but in contradiction with those of Horkay et al.[4] and Liu et al.[1] When the mesh size was significantly less than the linear chain length, Liu et al. observed that the linear chains segregated and formed a metastable state. They suggested that this behavior occurred because the linear chains could no longer stay homogeneously dispersed in the network and consequently aggregated in regions of lower cross-link density. Their observations imply that in order to see a decrease in R_g, a metastable state may need to be approached. In this study and in the work of Boué et al., the probe chains in the uncompressed 35K and 70K networks maintained Gaussian characteristics (as will be seen in the next section). Since these samples were formed by swelling the networks with the probe chains, it is believed a metastable state cannot be approached since the networks cannot be swollen "past equilibrium". Although the 10K samples were cross-linked in the presence of linear probe chains,
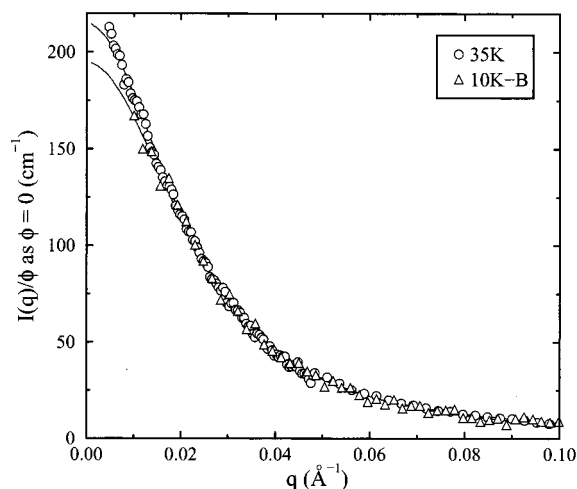
Figure 1. Zero concentration extrapolated scattering vs q for the 35K network and 10K-B blend series. The solid lines are the fits of eq 4.

the concentration of the linear probe chains was low and thermodynamic equilibrium was maintained.

The radius of gyration of the probe chains can also be extracted from the blend sample 70KB-1 using the single-chain form factor in the RPA equation (eq 9). In this case, the RPA equation with the parameters k_n, l, χ/v_0, and a baseline was coupled with the NREG library. Again, k_n was kept fixed and the baseline was fixed at zero, while l and χ/v_0 were allowed to float. In this algorithm, the degree of polymerization remains fixed at the value $N_1 = 580$ determined from extrapolating the other blend series (10KB) to infinite dilution. This is an alternate method for checking the radius of gyration and estimating the value for χ. For the 70KB-1 data, the RPA fit generates a value of 58.3 Å $\pm$ 0.3 Å for R_g ($l = 5.93$ Å $\pm$ 0.03 Å) and a χ value of 2.81×10^{-4} $\pm 1.07 \times 10^{-5}$. This R_g compares very well with that of the 10KB blends presented in Table 4. The χ value determined from the fit is considerably smaller than the value of $\chi = 1.7 \times 10^{-3}$ determined by Lapp et al.[41] However, their value was obtained by fitting apparent radii of gyration as a function of composition in fairly polydisperse mixtures and assuming a constant χ. The value of χ is now known to be composition dependent and fairly sensitive to the other fitting parameters.

Another method for determining the statistical segment length is by using a Kratky analysis, which is developed especially for the data in the high q range. Such an analysis of the data[32] leads to an estimate of $l = 6.1$ Å $\pm$ 0.1 Å ($R_g = 60$ Å $\pm$ 1 Å with $N_1 = 580$), only about 3% different from what was determined using the fit of the RPA equation. Although this method is less rigorous, it still provides a good estimate of l.

3.2. Compressed Networks. The samples that were compressed and the extent of their compression are presented in Table 2. One of the primary factors to contribute to the different results observed is believed to be phase separation and its kinetics. Therefore, after a description of the isointensity contour plots of the scattering, we will qualitatively compare the results of the different networks on the basis of evidence of phase separation under compression. We will then present a quantitative analysis of the results from the 10K networks where no evidence of phase separation was observed and for which the wormlike chain model provides a very good fit to the data.
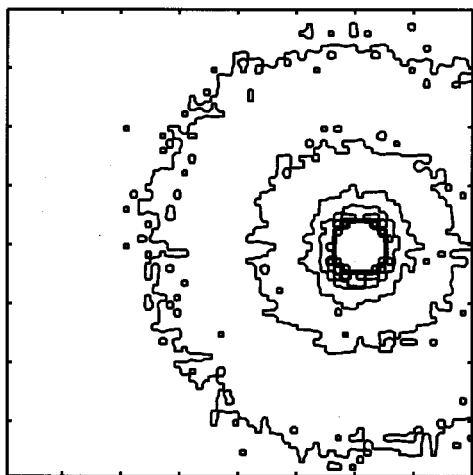
Figure 2. Isointensity contour plot of the scattering pattern of sample 35KC-5a. The detector was 64 cm × 64 cm at 30 m with wavelength $\lambda = 6$ Å. This figure corresponds to a q range of $0.0048-0.05$ Å^{-1}.
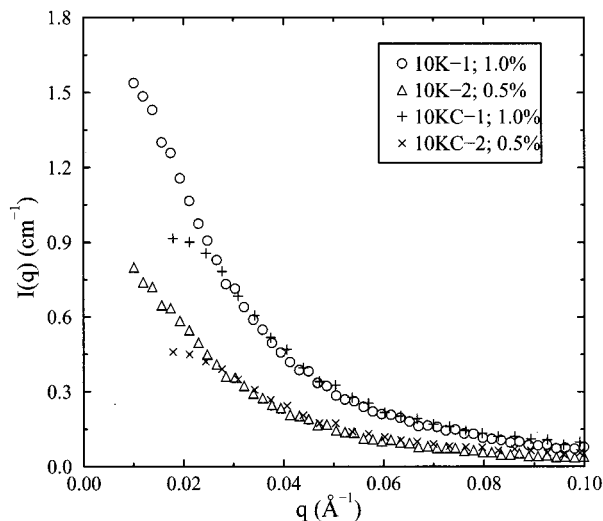

Figure 3. $I(q)$ vs q for the uncompressed and compressed 10K network series. The uncompressed samples are represented by open symbols, while the compressed samples are represented by $+$ and $\times$ symbols.

3.2.1. Isointensity Contour Plots. In Figure 2 the isointensity contours of the scattering pattern of the compressed 35KC-5a sample are presented. This scattering pattern appears isotropic as it should because the axis of compression was perpendicular to the wavevector q. Similar isotropic scattering patterns were observed for the other 35K and all of the 70K compressed (and uncompressed) samples. The isointensity contours of the scattering patterns of both the uncompressed and compressed 10K samples exhibited a slight amount of anisotropy. Similar anisotropic scattering was also observed in the scattering contours of the open neutron beam with no sample. Therefore, the anisotropy was determined to be an artifact of the neutron beam on the 8 m instrument at the time of the experiments.

During the data reduction process, the scattering data of the 10K samples were radially averaged. Averaging radially smooths out the effects of anisotropic scattering. While this scattering is not desirable, it should not affect the qualitative results significantly because the uncompressed sample scattering is compared to the compressed sample scattering, and both of them were subject to the same experimental artifact. Also, in the calculation of R_g of the probe chains in the uncompressed samples presented above, the radial averaging is expected to have reduced the effect of anisotropy.

3.2.2. Qualitative Comparison and Evidence of Phase Separation. A calculated equilibrium swelling curve ($\log(\phi_2)$ vs $\log(G_e/RT)$) of a PDMS network in a melt of linear PDMS chains can be obtained using the Flory–Rehner theory.[31] Using the experimentally determined elastic moduli (G_e/RT) of the dry networks presented in Table 1, the corresponding free chain volume fractions reported in Table 2, and the experimentally determined parameters of the chains, it is possible to determine the location of the samples relative to the calculated Flory–Rehner equilibrium swelling curve given by the swelling ratio (ϕ_2^{-1}) vs modulus. All the data points of the samples were found to lie in the one-phase region close to the calculated equilibrium swelling curve.[32]

Since the uncompressed samples lie close to the equilibrium swelling curve, when the network is compressed, the equilibrium swelling curve will shift downward depending on the amount of compression[42] push-

ing the sample into the two-phase region and potentially causing phase separation. It is very difficult to determine exactly where the equilibrium curve for each compressed sample would lie, but all of the samples will lie either close to or in the two-phase region when compressed.

The 10K series samples had the lowest fraction of deuterated material of all of the compressed samples and are therefore expected to remain in the one-phase region of the phase diagram. A plot of the scattering intensity vs scattering angle ($I(q)$ vs q) of the 10K compressed and uncompressed samples is shown in Figure 3. The scattering intensity does not appear to increase for the compressed samples. If the scattering intensity increased in the low q region, the probe chains would be exhibiting non-Gaussian behavior. The character of the probe chain can be further investigated by plotting the scattering data as $I(q)^{-1}$ vs q^2 or the Zimm representation of the data. The scattering of Gaussian chains in a single phase system should give a straight line on a plot of $I(q)^{-1}$ vs q^2, whereas non-Gaussian chains will show nonlinearity in the low q region.[1] The Zimm plot of the 10KU and 10KC networks is shown in Figure 4. The Zimm plots of the uncompressed as well as the compressed samples are linear, confirming that the chains are Gaussian. Despite the fact that data for the 10KC series could not be collected in the very low q region due to the experimental configuration, a combination of the $I(q)$ vs q and Zimm plots suggests that phase separation did not occur in these samples. Another way to present differences in the scattering data between compressed and uncompressed samples is using the Kratky representation of the data, $I(q)q^2$ vs q. The Kratky plots of the 10KU and 10KC samples are shown in Figure 5. The plots of the uncompressed samples are relatively constant at high q and are a corroboration that the probe chains exhibit Gaussian behavior. On the other hand, an unusual effect is observed in this figure for the compressed samples 10KC-1 and 10KC-2. The data for these samples show a crossover from Gaussian behavior to rodlike behavior in the medium to high q range. This upturn in the Kratky plot is an indication that the probe chains in the compressed network are stiffer at small distances
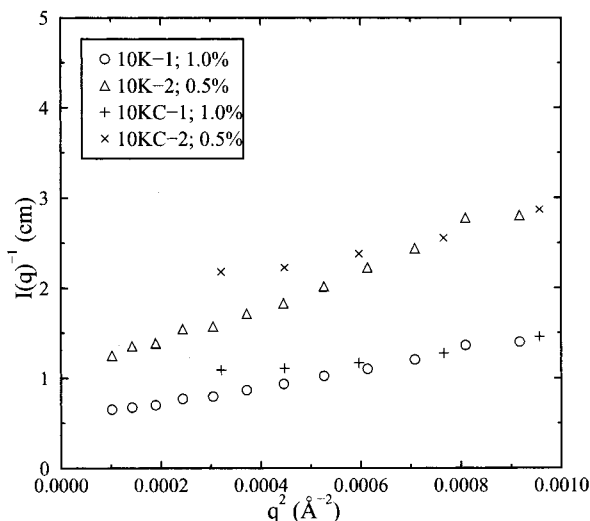
Figure 4. $I(q)^{-1}$ vs q^2 for the compressed 10K network samples and their corresponding uncompressed samples. The uncompressed samples are represented by open symbols, while the compressed samples are represented by + and × symbols.
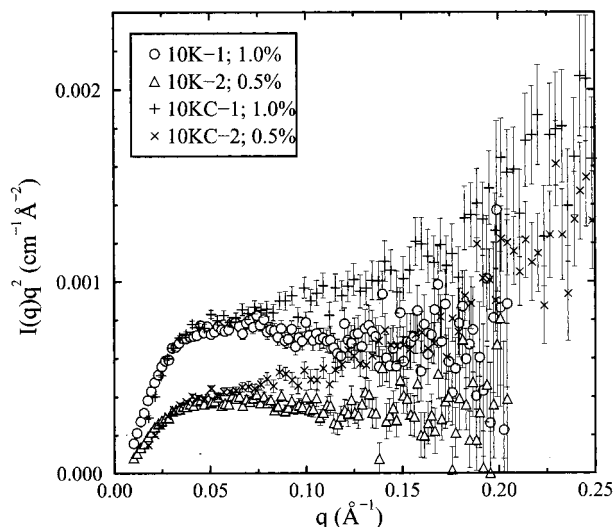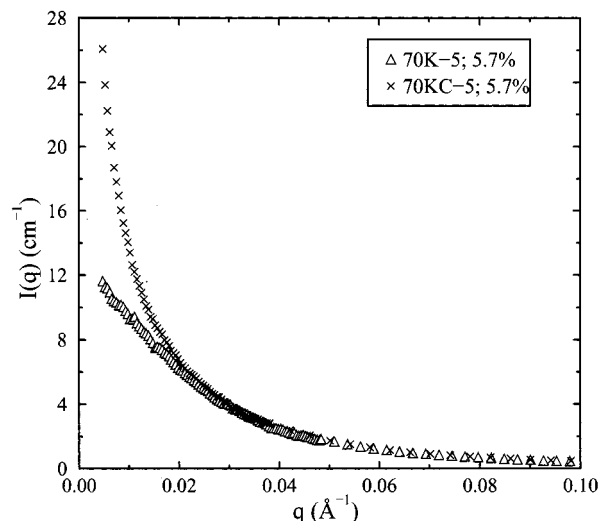

Figure 6. $I(q)$ vs q for the compressed 70K network sample and its corresponding uncompressed sample. The uncompressed sample is represented by an open symbol, while the compressed sample is represented by the × symbol.
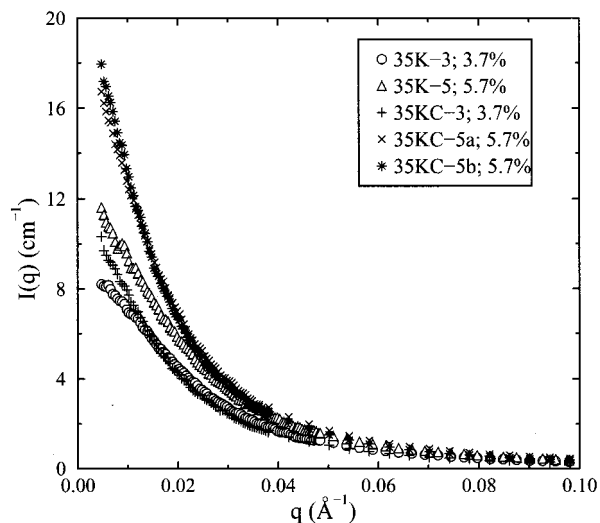

Figure 5. $I(q)q^2$ vs q for the compressed 10K network samples and their corresponding uncompressed samples. The uncompressed samples are represented by open symbols, while the compressed samples are represented by + and × symbols.

Figure 7. $I(q)$ vs q for the compressed 35K network samples and their corresponding uncompressed samples. The uncompressed samples are represented by open symbols, while the compressed samples are represented by +, ×, and * symbols.

relative to their Gaussian structure in the uncompressed network.

The 10K networks did not exhibit signs of phase separation. Such signs were evident, however, in the case of the 35K and 70K networks. In microsyneresis, phase separation occurs within the network and the linear chains aggregate and microphase separate locally inside the network.[43] Microphase separation in the networks creates a heterogeneous system that shows increased scattering at low q.

The $I(q)$ vs q plots of the uncompressed and corresponding compressed samples of the 70K and 35K series are shown in Figures 6 and 7, respectively. In the low q region, the compressed samples display a dramatic increase in scattering intensity compared to the uncompressed samples. Deformed polymer networks often show increased scattering in the low q region, indicating that the chains are exhibiting non-Gaussian behavior. Bastide et al.[18] suggested that fluctuations in the cross-link density are magnified during deformation, causing

increased scattering. Another explanation for the increased neutron scattering upon compression of the samples is that of increased concentration fluctuations due to microphase separation or an approach to a phase boundary. This increased scattering can be further investigated by examining the Zimm plots of the scattering data, an example of which is shown in Figure 8 for the 70K-5 sample. The scattering of the uncompressed sample is linear in the low q region, whereas the scattering of the compressed sample is decidedly nonlinear. Furthermore, although the Kratky plot of these data, shown in Figure 9, exhibits an upturn in the medium to high q range as in the case of the 10K networks, we will show that these data cannot be fitted to a simple model such as the wormlike chain. These behaviors therefore suggest that the 70KC-5 sample underwent microsyneresis under compression. Although the Zimm plots of the 35K compressed networks appeared to be relatively linear, the Kratky representations of these results exhibited different and inconsistent behavior.[32] We suspect that a factor that may have
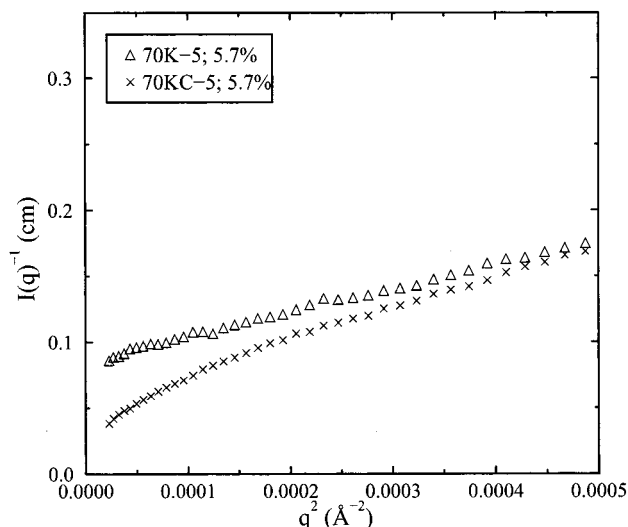
Figure 8. $I(q)^{-1}$ vs q^2 for the compressed 70K network sample and its corresponding uncompressed sample. The uncompressed sample is represented by an open symbol, while the compressed sample is represented by the $\times$ symbol.
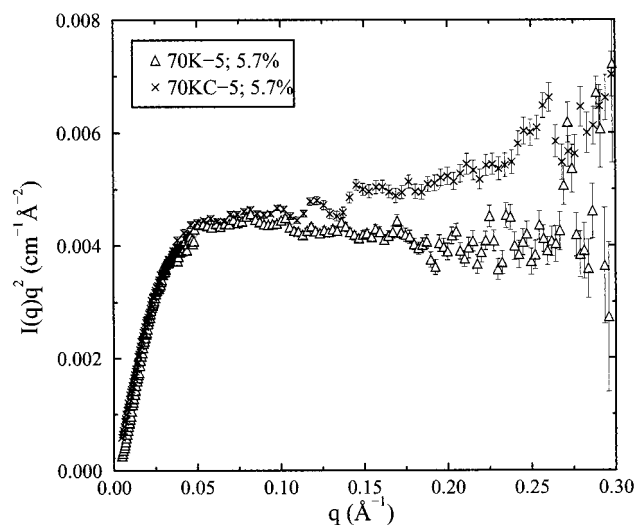

Figure 9. $I(q)q^2$ vs q for the compressed 70K network sample and its corresponding uncompressed sample. The uncompressed sample is represented by an open symbol, while the compressed sample is represented by the $\times$ symbol.

contributed to the different scattering behavior of the different samples is the kinetics of phase separation that was not taken into account in our experiments. There was, for example, an approximate 17 h time delay between the first and second compression of sample 35K-5. It is postulated that under compression (see Table 2) the probe chains in these samples were exuded from the samples (macrosyneresis). Such a behavior was also observed while performing deuterium NMR measurements of similar samples under compression.[44]

3.2.3. Quantitative Analysis Using the Wormlike Chain Model. Assuming that the 10K networks remained in a single phase when compressed, we now analyze the data of the 10K networks in terms of probe chains that become stiffer as the surrounding network is strained. Supporting evidence for such behavior comes from D NMR results from probe chains in compressed and stretched networks[13−17] as well as from computer simulations showing increased orientation correlation of the probe chain segments.[5−12]
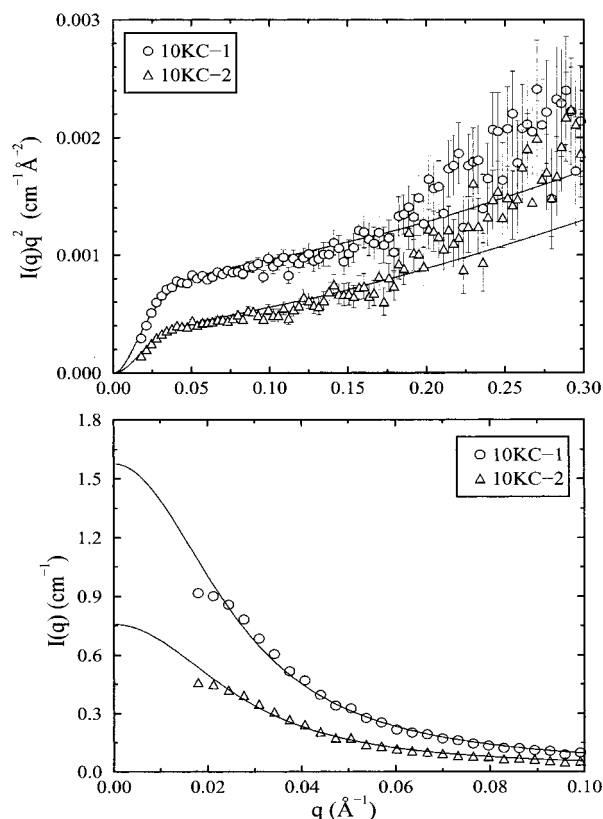

Figure 10. (a) $I(q)q^2$ vs q for the compressed 10K network samples. The solid lines are fits from the Kratky−Porod wormlike chain model. (b) $I(q)$ vs q representation of the data above.

A chain that is stiffer, or semiflexible, can be modeled using the Kratky−Porod (KP) wormlike chain model as described in the Appendix by eqs 1−9 along with the relations for the polydisperse single-chain form factor, $P_{1,P}$, given by eqs 5−7.

The scattering data from the compressed samples in a given series could not be extrapolated to infinite dilution because the samples were not compressed to the same degree, thus preventing the use of eq 4. Instead, the single-chain form factor for the KP chain was used in eq 1, which introduced another parameter, A_2. Equation 1 in Kratky form is

$$I(q)q^2 = q^2\left[\frac{1}{k_n v_1 N_1 \phi_1 P_{1,KP}} + 2\frac{A_2}{k_n}\right]^{-1} \quad (12)$$

where $P_{1,KP}$ is given by eqs A2−A9. The variable parameters are the contour length L, the Kuhn length b, the number-average degree of polymerization N_1, and the second virial coefficient A_2. The program used to determine the best-fit values of these variable parameters was coupled again with the NREG libraries.[36] It is advantageous to keep at least one parameter fixed, and N_1 is the most appropriate to keep constant as it can be obtained from the extrapolation to infinite dilution of the uncompressed networks. Since there is a considerable amount of uncertainty in the data at high q, a weighting function was applied to the fit such that experimental data with larger error were weighted proportionally less in determining the fit. The values of the fitted parameters are identical whether $I(q)q^2$ vs q data or $I(q)$ vs q data are fit.

The best fits to the scattering data from samples 10KC-1 and 10KC-2 are shown in Figure 10. The top
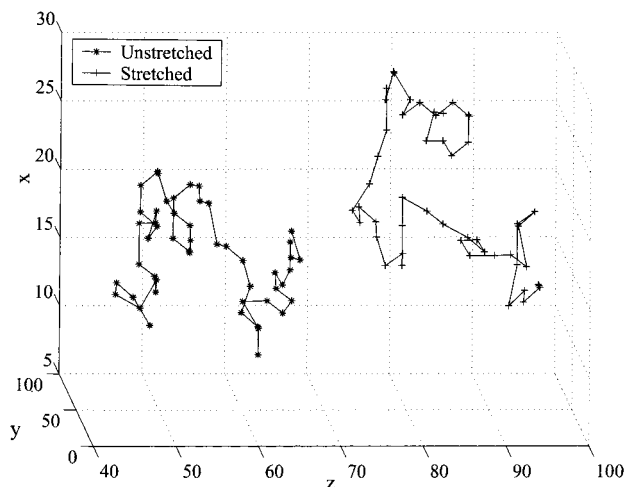
Figure 11. Figure of one linear probe chain in an unstretched and stretched polymer network generated by Monte Carlo simulations. The units of the x, y, and z axes are lattice constants.

figure shows the KP fit, and the lower figure shows the representation of the data in the $I(q)$ vs q form. For all fits, a constant value of $N_l = 580$ was used. Good agreement between the KP fit and the data is seen for both the Kratky and the $I(q)$ vs q plots for the 10KC series. The deviation of the $I(q)$ vs q fit from the first two data points at low q, shown in Figure 4b, occurs because these data are near the beamstop and, therefore, are not significant in this analysis.

The average contour length of the probe chains in samples 10KC-1 and 10KC-2 determined using the Kratky–Porod model is 776 ± 35 Å. The Kuhn length of a PDMS chain in the melt is 15.6 Å.[46] It can be seen that the Kuhn length of samples 10KC-1 and 10KC-2, 23.4 Å ± 0.8 Å and 36.5 Å ± 1.7 Å, respectively, are considerably greater than that of the unperturbed chain, indicating that the chains in those samples are stiffer. Furthermore, it can be seen from Table 5 that the Kuhn length of the KP chains in the samples increases with increasing amount of compression. As the amount of compression is increased by approximately 45%, the Kuhn length increases approximately 40%. Also, the radii of gyration of the KP chains are roughly equivalent to their uncompressed, Gaussian counterparts. This suggests that the KP chains are remaining Gaussian on large length scales. The overall Gaussian nature of the chain is maintained with the same average radius of gyration by involving fewer but larger Kuhn steps. This is illustrated in Figure 11 showing the configuration of a free chain in a network obtained from Monte Carlo simulations using the bond-fluctuation model.[46,47] The configuration on the left is that of the probe chain in an undeformed network, and the configuration on the right is that of the same chain under uniaxial expansion in the z-direction of the network with an extension ratio of $\lambda = 2.65$. Details of the simulation are given elsewhere.[48] Although the radius of gyration of the chain remained essentially unchanged, the chain in the deformed network clearly shows that the orientation of neighboring segments of the chain in the deformed network is more highly correlated than in the unde-formed network.[48] The increased chain rigidity exhibited in the KP plots of Figure 11 and in the computer simulation results of Figure 11 is also likely to be the origin of the orientation correlations observed by D NMR.
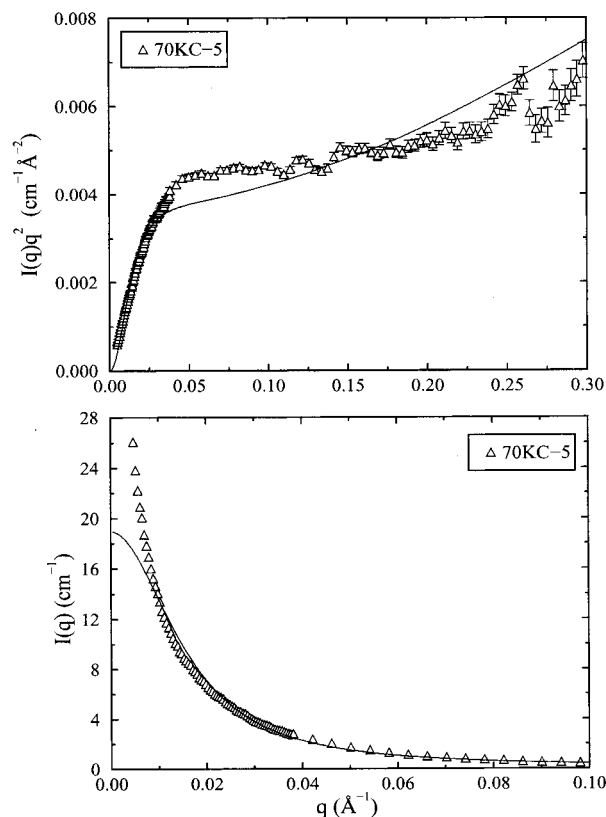

Figure 12. (a) $I(q)q^2$ vs q for the compressed 70K network sample. The solid line is a fit from the Kratky–Porod wormlike chain model. (b) $I(q)$ vs q representation of the data above.

Table 5. L, b, R_g, and A_2 As Determined by a Nonlinear Fit of the Compressed Samples Using the Kratky–Porod Wormlike Chain Model[a]

sample	L (Å)	b (Å)	R_g (Å)	$A_2 \times 10^5$ (cm^3/mol)
10KC-1	947.7 ± 27.7	23.4 ± 0.8	59.7 ± 1.3	21.9 ± 7.1
10KC-2	604.9 ± 20.9	36.5 ± 1.7	58.0 ± 1.6	52.6 ± 16
35KC-5a[b]	1156.5 ± 9.5	24.8 ± 0.2	68.1 ± 0.4	-5.20 ± 0.11
70KC-5[b]	1223.1 ± 36.6	24.5 ± 0.8	69.6 ± 1.2	-6.30 ± 0.39

[a] For all samples, $N_l = 580$. [b] The linear probe chains have segregated in these samples.

Attempts to fit the Kratky plots from the 35K and 70K networks with the KP model were unsuccessful. Figure 12 show an example of the best possible fit obtained for the 70KC-5 network. Although the fit parameters of the KP model are not meaningful in these samples that are phase separated or near phase separation, it is interesting to note from Table 5 that the best-fit values of the second virial coefficient, A_2, are negative for these samples. This implies unfavorable thermodynamic conditions. On the other hand, the A_2 values extracted from the good fits to the results from the 10KC samples are positive.

4. Conclusions

In this study, the conformation of free probe PDMS chains in both uncompressed and compressed PDMS networks was examined using small-angle neutron scattering. Three series of end-linked PDMS networks with a minimal amount of defects and mesh sizes of M_n = 9900 g mol^{-1}, 34 800 g mol^{-1}, and 71 500 g mol^{-1} were examined containing low volume fractions of deuterated, linear M_n = 51 000 g mol^{-1} PDMS. Two series of binary

blends of these probe chains with protonated PDMS chains of M_n = 9900 and 71 500 g mol^{-1} were also studied.

The radius of gyration of the probe chains was determined by extrapolating the scattering data of each series to infinite dilution and using a nonlinear fitting routine. It was determined that R_g of the PDMS chains in the networks varied in the range 60 Å−65 Å and did not appear to be a strong function of the network mesh size, since the R_g of the chains in the blend was measured to be in the range 58 Å−59 Å.

The effect of compression on the conformation of the probe chains was also studied. Here the results are not as clear-cut, primarily because of the tendency of phase segregation of the probe chains in the compressed networks. In both the 35KC and 70KC samples, an increased scattering at small q was observed, and the results could not be quantitatively modeled. For the case of the 10KC samples, which are believed to have remained homogeneous under compression, a good fit of the data to the Kratky−Porod wormlike chain model was obtained, and a contour length L = 776 Å ± 35 Å was determined. Also, the Kuhn length was greater for the probe chains in these samples under compression than for the same chain in the melt, indicating that compressing the samples induced rigidity in the probe chains. The Kuhn length was found to be a function of the amount of compression: as the amount of compression was increased by approximately 45%, the Kuhn length increased by approximately 40%. Furthermore, the probe chains in these compressed 10KC series samples maintained the same radius of gyration as that of the uncompressed samples. Because the KP wormlike model used gives a reasonable fit of the data and assumes Gaussian behavior at long distances and rodlike behavior at short distances, it would imply that the probe chains in the deformed networks remain Gaussian at long distances but their stiffness increases at short distances. This conclusion is supported by computer simulation results. The increased local chain alignment at short length scales is also likely to be related to the increased orientation correlation observed by D NMR.

Appendix

The Kratky−Porod (KP) wormlike chain can be fully described using two model parameters: the contour length, L, and the Kuhn length, b. For purposes of simplification, the following equations are presented in terms of the contour length and a reduced length Z, where $Z = L/b$.

The mean-squared radius of gyration of a wormlike chain is[49]

$$\langle R_g^2 \rangle = b^2 \left[\frac{Z}{6} - \frac{1}{4} + \frac{1}{4Z} - \frac{1}{8Z^2}(1 - e^{-2Z}) \right] \quad \text{(A1)}$$

The scattering function of a Kratky−Porod wormlike chain, $P_{1,KP}(q;Z)$, can be modeled using a formula that interpolates between the Gaussian and rodlike regimes developed by Yamakawa et al.[50,51] The interpolation formula is given by

$$P_{1,KP}(q;Z) = P_0(q;Z)\, \Gamma(q;Z) \quad \text{(A2)}$$

where P_0 is given by

$$P_0(q;Z) = [1 - \tau(q;Z)]P_G(q;Z) + \tau(q;Z)\, P_R(q;L) \quad \text{(A3)}$$

where $P_G(q;Z)$ is the scattering function for a polydisperse Gaussian chain described by eqs 5−7. $P_R(q;L)$ is the scattering function for an infinitely thin, monodisperse rod[34]

$$P_R(q;L) = 2v^{-2}[v\int_0^v t^{-1}\sin t\, dt + \cos v - 1] \quad \text{(A4)}$$

with $v = Lq$. The function $\tau(q;Z)$ is defined as

$$\tau(q;Z) = \exp(-\xi^{-5}) \quad \text{(A5)}$$

with

$$\xi(q;Z) = \frac{\pi\langle R_g^2 \rangle q}{2L} \quad \text{(A6)}$$

In eq 2, $\Gamma(q;Z)$ is given by

$$\Gamma(q;Z) = 1 + (1 - \tau)\sum_{i=2}^{5}A_i\xi^i + \tau\sum_{i=0}^{2}B_i\xi^{-i} \quad \text{(A7)}$$

with

$$A_i = \sum_{j=0}^{2}a_{1,ij}Z^{-j}e^{-10/Z} + \sum_{j=1}^{2}a_{2,ij}Z^{-j}e^{-2Z} \quad \text{(A8)}$$

$$B_i = \sum_{j=0}^{2}b_{1,ij}Z^{-j} + \sum_{j=1}^{2}b_{2,ij}Z^{j}e^{-2Z} \quad \text{(A9)}$$

where $a_{1,ij}$, $a_{2,ij}$, $b_{1,ij}$, and $b_{2,ij}$ are numerical coefficients determined by Yamakawa.[50] The application of these equations to model the Kratky−Porod wormlike chain are valid only for $qb \leq 10$. Additional explanations and details can be found elsewhere.[28,32,50]

References and Notes

(1) Liu, X.; Bauer, B.; Briber, R. *Macromolecules* **1997**, *30*, 4704−4712.
(2) Briber, R.; Liu, X.; Bauer, B. *Science* **1995**, *268*, 395−397.
(3) Boué, F.; Farnoux, B.; Bastide, J.; Lapp, A.; Herz, J.; Picot, C. *Europhys. Lett.* **1986**, *12*, 637−645.
(4) Horkay, F.; Stanley, H.; Geissler, E.; King, S. *Macromolecules* **1995**, *28*, 678−681.
(5) Yong, C.; Higgs, P. *Macromolecules* **1999**, *32*, 5062−5071.
(6) Sotta, P. *Macromolecules* **1998**, *31*, 8417−8422.
(7) Baljon, A.; Grest, G.; Witten, T. *Macromolecules* **1995**, *28*, 1835−1840.
(8) Gao, J.; Weiner, J. *Macromolecules* **1991**, *24*, 5179−5191.

(9) Depner, M.; Deloche, B.; Sotta, P. *Macromolecules* **1994**, *27*, 5192−5199.

(10) Haslam, A.; Jackson, G.; McLeish, T. *Macromolecules* **1999**, *32*, 7289−7298.

(11) Edwards, S.; McLeish, T. *J. Chem. Phys.* **1990**, *92*, 6855−6857.

(12) Sotta, P.; Higgs, P.; Depner, M.; Deloche, B. *Macromolecules* **1995**, *28*, 7208−7214.

(13) Gronski, W.; Stadler, R.; Jacobi, M. *Macromolecules* **1984**, *17*, 741−748.

(14) Brereton, M. *Macromolecules* **1993**, *26*, 1152−1157.

(15) Brereton, M.; Ries, M. *Macromolecules* **1996**, *29*, 2644−2651.

(16) Ylitalo, C.; Zawada, J.; Fuller, G.; Abetz, V.; Stadler, R. *Polymer* **1992**, *33*, 2949−2960.

(17) Sotta, P.; Deloche, B.; Herz, J.; Lapp, A.; Durand, D.; Rabadeux, J.-C. *Macromolecules* **1987**, *20*, 2769−2774.

(18) Bastide, J.; Leibler, L.; Prost, J. *Macromolecules* **1990**, *23*, 1821−1825.

(19) Oeser, R. *Prog. Colloid Polym. Sci.* **1992**, *90*, 131−136.

(20) Horkay, F.; Hecht, A.-M.; Geissler, E. *Macromolecules* **1998**, *31*, 8851−8856.

(21) Boué, F.; Bastide, J.; Buzier, M.; Collette, C.; Lapp, A.; Herz, J. *Prog. Colloid Polym. Sci.* **1987**, *75*, 152−170.

(22) Patel, S.; Malone, S.; Cohen, C.; Gillmor, J.; Colby, R. *Macromolecules* **1992**, *25*, 5241−5251.

(23) McLoughlin, K.; Szeto, C.; Duncan, T.; Cohen, C. *Macromolecules* **1996**, *29*, 5475−5483.

(24) Gilra, N.; Cohen, C.; Panagiotopoulos, A. *J. Chem. Phys.* **2000**, *112*, 6910−6916.

(25) Mori, K.; Tanaka, H.; Hagesawa, H.; Hashimoto, T. *Polymer* **1989**, *30*, 1389−1398.

(26) Debye, P. *J. Phys. Colloid Chem.* **1947**, *51*, 18−32.

(27) Pedersen, J. *Adv. Colloid Interface Sci.* **1997**, *70*, 171−210.

(28) Fujita, H. *Polymer Solutions;* Elsevier Science: New York, 1990.

(29) de Gennes, P.-G. *Scaling Concepts in Polymer Physics;* Cornell University Press: Ithaca, NY, 1979.

(30) Lapp, A.; Herz, J.; Strazielle, C. *Makromol. Chem.* **1985**, *186*, 1919−1934.

(31) Gent, A.; Tobias, R. *J. Polym. Sci., Polym. Phys. Ed.* **1982**, *20*, 2317−2326.

(32) Gilra, N. Ph.D. Thesis, Cornell University, 2000.

(33) Certain commercial materials and equipment are identified in this paper to specify adequately the experimental procedure. In no case does such identification imply recommendation by the National Institute of Standards and Technology nor does it imply that the material or equipment identified is necessarily the best available for this purpose.

(34) Higgins, J.; Benoît, H. *Polymers and Neutron Scattering;* Oxford University Press: Oxford, 1994.

(35) Jinnai, H.; Briber, R. FORTRAN program for nonlinear fitting using the dilute Zimm theory and the RPA equation, University of Maryland, College Park.

(36) NREG: Nonlinear regression routine, University of Wisconsin, Madison, 1979.

(37) Flory, P. *Statistical Mechanics of Chain Molecules;* Wiley-Interscience: New York, 1969.

(38) Beaucage, G.; Sukumaran, S.; Clarson, S.; Kent, M.; Schaefer, D. *Macromolecules* **1996**, *29*, 8349−8356.

(39) Schulz, G.; Haug, A. *Z. Phys. Chem.* (*Munich*) **1962**, *34*, 328−349.

(40) Gilra, N.; Panagiotopoulos, A.; Cohen, C. *J. Chem. Phys.* **2001**, *115*, 1100−1104.

(41) Lapp, A.; Picot, C.; Benoît, H. *Macromolecules* **1985**, *18*, 2437−2445.

(42) Bauer, B.; Briber, R.; Han, C. *Macromolecules* **1989**, *22*, 940−948.

(43) Dušek, K.; Prins, W. *Adv. Polym. Sci.* **1969**, *6*, 1−102.

(44) Hedden, R. PhD Thesis, Cornell University, 2000.

(45) Shibanov, Y.; Karpov, L. *Polym. Sci.* **1989**, *31*, 2653−2662.

(46) Deutsch, H.-P.; Binder, K. *J. Chem. Phys.* **1991**, *94*, 2294−2304.

(47) Paul, W.; Binder, K.; Heermann, D.; Kremer, K. *J. Phys. II* **1991**, *1*, 37−60.

(48) Gilra, N.; Panagiotopoulos, A.; Cohen, C. *Macromolecules* **2001**, *34*, 6090−6096.

(49) Benoît, H.; Doty, P. *J. Phys. Chem.* **1953**, *57*, 958−963.

(50) Yamakawa, H. *Helical Wormlike Chains in Polymer Solutions;* Springer-Verlag: Berlin, 1997.

(51) Yoshizaki, T.; Yamakawa, H. *Macromolecules* **1980**, *13*, 1518−1525.